I&EC research
Industrial & Engineering Chemistry Research

Article

pubs.acs.org/IECR

Photocatalytic Reduction of Cr(VI) in an Aqueous Suspension of Surface-Fluorinated Anatase TiO_2 Nanosheets with Exposed {001} Facets

Zhiqiao He, Qiaolan Cai, Ming Wu, Yuanqiao Shi, Huiying Fang, Lingdan Li, Jiancheng Chen, Jianmeng Chen, and Shuang Song*

College of Biological and Environmental Engineering, Zhejiang University of Technology, Hangzhou 310032, People's Republic of China

ABSTRACT: In the present work, reduction of Cr(VI) induced by UV−visible light in aqueous solution was investigated. The aqueous medium contained TiO_2 nanosheets and no additional reducing agents or hole scavengers. A hydrothermal method was used to synthesize fluorinated TiO_2 nanostructures with various percentages of exposed {001} facets and initial F/Ti ratios. Fluorine-free TiO_2 nanosheets were obtained by washing the TiO_2 samples with NaOH solution. The surface fluorination facilitates the adsorption process by increasing the number of surface OH groups generated. Moreover, fluorination efficiently inhibits the recombination of photogenerated electron−hole pairs. The {001} facets have an indirect role in the photocatalytic reduction of Cr(VI) because oxidative dissolution of H_2O occurring on {001} facets and Cr(VI) reduction occurring on {101} facets are simultaneous reactions. The optimal ratio of exposed {001} to {101} was found to be ~72:18.

1. INTRODUCTION

Hexavalent chromium (Cr(VI)) is one of the forms of chromium that poses a health risk to humans because of its high acute toxicity and carcinogenic activity. This species is generally released in effluent in various industrial activities, including electroplating, leather tanning, metal finishing, dyeing, textile production, and steel fabrication. Other applications that involve paint and pigments, fertilizer use, and photography also have potential to release Cr(VI) into the environment.[1−5] Trivalent chromium (Cr(III)) is another form of chromium that is much less toxic and less mobile than Cr(VI). It can be easily removed from wastewater as a solid by alkalinification and precipitation. Thus, development of effective technologies to reduce Cr(VI) to Cr(III) is of great importance in the treatment of wastewater and water for consumption.

Various innovative technologies proposed for the conversion of Cr(VI) to Cr(III) include reduction by chemical reducing agents (ferrous sulfate, sodium pyrosulfite, sodium hydrogen sulfite, hydrazine hydrate, or sulfur dioxide), microbial reduction, and photocatalytic reduction.[1−7] Among these, solar photocatalysis using semiconductors is an efficient, dynamic, and clean technology; it does not use or release hazardous chemicals.

Photocatalytic reduction of Cr(VI) is a surface reaction mediated by the electrostatic attraction between positively charged surface $-OH_2^+$ groups and negatively charged CrO_4^{2-} or $Cr_2O_7^{2-}$ groups.[8,9] A plausible chemical reaction of the photocatalytic reduction of Cr(VI) is represented as follows:[10,11]

$$\text{photocatalyst} + h\nu \rightarrow TiO_2(e^- + h^+) \quad (1)$$

$$Cr_2O_7^{2-} + 14H^+ + 6e^- \rightarrow 2Cr^{3+} + 7H_2O \quad (2)$$

$$2H_2O + 4h^+ \rightarrow O_2 + 4H^+ \quad (3)$$

TiO_2 is the most frequently used catalyst in the photocatalytic reduction of Cr(VI) because of its favorable physical/chemical properties, high stability, and relatively low cost.[12,13] The exposed facets in the crystal play a crucial role in determining the photocatalytic reactivity and efficiency,[14,15] as photocatalytic reactions usually occur on the surfaces of semiconductors.[16] For anatase TiO_2 nanocrystals, different facets exhibit distinct activities because their surface energies are different. The order of the average surface energies is γ{110} (1.09 J m^{-2}) > γ{001} (0.90 J m^{-2}) > γ{100} (0.53 J m^{-2}) > γ{101} (0.44 J m^{-2}).[17−19] However, most available anatase TiO_2 nanocrystals are mainly dominated by the thermodynamically stable {101} facets rather than the more reactive {001} facets.[20] Hence, many studies have focused on the method of preparing TiO_2 nanosheets with exposed {001} facets and their application in the photocatalytic degradation of organic pollutants.[21−26] To date, studies on photocatalytic reduction using TiO_2 nanosheets with exposed {001} facets are few. Consequently, it is highly desirable to investigate the capability of TiO_2 nanosheets with high levels of exposed {001} facets in the reduction of Cr(VI) in water.

Catalytic activity for the photoreduction of Cr(VI) is also strongly dependent on the surface OH groups, since they are the adsorption sites for the negatively charged Cr(VI).[8,9] Photocatalysts with more surface OH groups are expected to facilitate the adsorption of Cr(VI) on the TiO_2 surface and thereby enhance reduction. {001} facet is beneficial to the dissociation of water into two hydroxyl groups.[24] Moreover,

Received: March 13, 2013
Revised: May 26, 2013
Accepted: June 12, 2013
Published: June 12, 2013

dx.doi.org/10.1021/ie400812m | *Ind. Eng. Chem. Res.* 2013, 52, 9556−9565

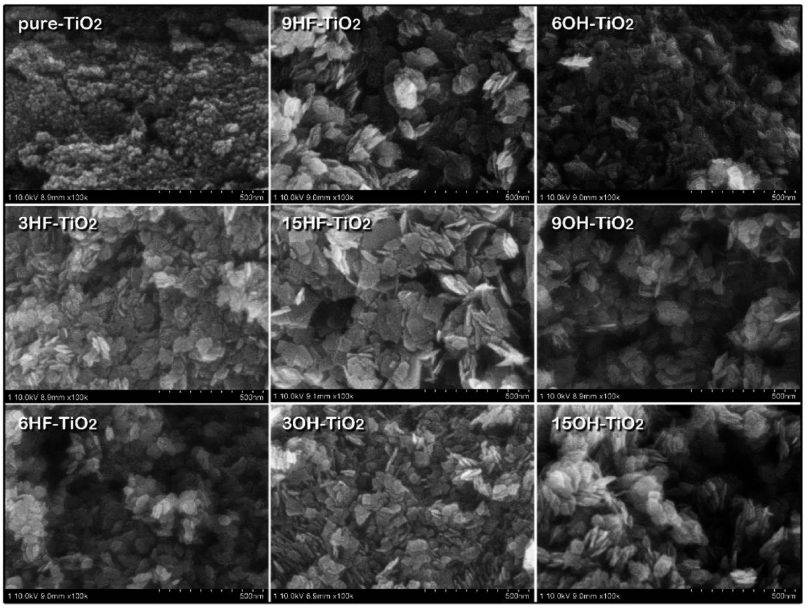

Figure 1. FESEM images of pure-TiO_2, 3HF-TiO_2, 6HF-TiO_2, 9HF-TiO_2, 15HF-TiO_2, 3OH-TiO_2, 6OH-TiO_2, 9OH-TiO_2, and 15OH-TiO_2.

synthesis of anatase TiO_2 with high proportions of {001} facets often employs fluorine-containing compounds such as hydrofluoric acid as morphology-controlling agents, leading to a process known as surface fluorination.[22] Our earlier works have demonstrated that surface fluorination can facilitate conversion of Ti^{4+} to Ti^{3+} mainly by charge compensation.[27] As a result, the fluorinated titanium surfaces have high hydrophilicity and thus great ability to adsorb oxygen and water molecules, favoring the formation of surface OH groups. Therefore, the dependence of photocatalytic reduction of Cr(VI) on the presence of surface OH groups deserves special attention. In this respect, formation of OH groups induced by exposure of the {001} facets and surface fluorination is also of interest.

Surface-fluorinated TiO_2 nanosheets with dominant {001} facets hold promise in producing catalysts that enhance the photoreduction of Cr(VI) in aqueous solution. This potential is due to their surface fluorination and exposed {001} facets (which improve the photocatalytic activity) and the surface OH groups (which play a predominant role in the adsorption of Cr(VI)). In this study, surface-fluorinated TiO_2 catalysts with various proportions of exposed {001} facets were fabricated via a hydrothermal method using tetrabutyl titanate ($Ti(OC_4H_9)_4$) as the titanium source and HF solution as the suspending medium The catalysts were used in the photoreduction of Cr(VI) under UV−visible light irradiation in aqueous solution, without adding additional reducing agents or hole scavengers. The percentage of {001} facets and the concentration of surface OH groups were quantified to study the effects of exposed crystal facets and surface fluorination on the photocatalytic activity.

2. EXPERIMENTAL SECTION

2.1. Reagents. Potassium dichromate ($K_2Cr_2O_7$, 99.9%) was purchased from Wuxi Haishuo Biology Co., Ltd. (Wuxi, China). Absolute ethanol (99.5%), $Ti(OC_4H_9)_4$, and HF solution (40 wt %) for the preparation of the TiO_2 nanosheets were obtained from Huadong Medicine Co., Ltd. (Hangzhou, China). Concentrated H_2SO_4 (98 wt %), 1,5-diphenylcarbazide (DPC, 98%), $KMnO_4$ (99.5%), and acetone were from Aladdin Reagent Co., Ltd. (Shanghai, China). All materials were used without further purification. Distilled deionized water was used throughout this work.

2.2. Preparation and Characterization of TiO_2. The TiO_2 nanosheets were synthesized via a facile hydrothermal method similar to that described elsewhere.[22] A mixture of 50 mL of $Ti(OC_4H_9)_4$ and an appropriate amount of concentrated HF was transferred to a 200 mL Teflon-lined stainless steel autoclave, heated at 180 °C for 24 h, and then allowed to cool down to room temperature. The resulting white precipitate was harvested by centrifugation and washed with absolute ethanol and then with water several times, and finally dried at 60 °C for 10 h before characterization. The nomenclature used for the catalysts is *n*HF-TiO_2, where *n* is the amount of concentrated HF added (in mL). The white precipitates obtained after the hydrothermal treatments were further washed with 0.1 M NaOH to replace the F^- groups with hydroxyl groups. The resulting samples are denoted as *n*OH-TiO_2. For comparison, control samples of pure-TiO_2 were prepared by using 6 mL of H_2O instead of 6 mL of HF under the same conditions.

To identify the crystallization level and crystal phase of the catalysts, X-ray diffraction (XRD) was performed with a Thermo ARL diffractometer (model X'TRA 17) using a Cu Kα radiation source operated at 45 kV and 40 mA over the 2θ range 20°−80°. Field-emission scanning electron microscopy (FESEM) was done using a Hitachi model S-4800 instrument to view the morphology of the TiO_2 samples. Transmission electron microscopy (TEM) was done on an FEI Tecnai instrument (model G2 F-30) to analyze the microstructure of the products. The instrument was operated at 300 kV accelerating voltage and 0.2 nm point resolution. To measure the elemental composition, chemical state, and electronic state of the elements present on the surface of the samples, X-ray photoelectron spectroscopy (XPS) was performed using an RBD upgraded PHI-5000C ESCA system (PerkinElmer) equipped with a polychromatic Mg Kα radiation source operated at 1253.6 eV. The surface area of the samples was measured using a Brunauer−Emmett−Teller (BET) analyzer (Micromeritics ASAP 2010). The pore size distribution of the

dx.doi.org/10.1021/ie400812m | *Ind. Eng. Chem. Res.* 2013, 52, 9556−9565

Table 1. Summary of Physicochemical Parameters of Various Photocatalysts and the Pseudo-First-Order Rate Constants for the Reduction of Cr(VI)

catalysts	S_{BET} (m^2 g^{-1})	crystallite phase (%)	concentration of surface OH (mmol g^{-1})	pore diameter (nm)	percentage of {001} (%)	dark adsorption for Cr(VI) (mg g^{-1})	$k \times 10^2$ (min^{-1})
pure-TiO_2	197	A100	0.613	5.3	<10 ± 1	0.825	0.76
3HF-TiO_2	160	A100	1.073	5.6	67 ± 4	1.665	2.62
6HF-TiO_2	136	A100	1.208	11.1	76 ± 4	1.935	5.37
9HF-TiO_2	130	A100	1.267	15.4	80 ± 4	2.010	4.46
15HF-TiO_2	97	A100	1.407	27.3	83 ± 4	2.190	3.42
3OH-TiO_2	180	A100	0.845	10.3	65 ± 5	1.185	0.81
6OH-TiO_2	149	A100	0.962	12.3	72 ± 5	1.425	3.72
9OH-TiO_2	137	A100	1.152	18.2	77 ± 5	1.770	1.92
15OH-TiO_2	135	A100	1.195	21.3	81 ± 5	1.845	1.10

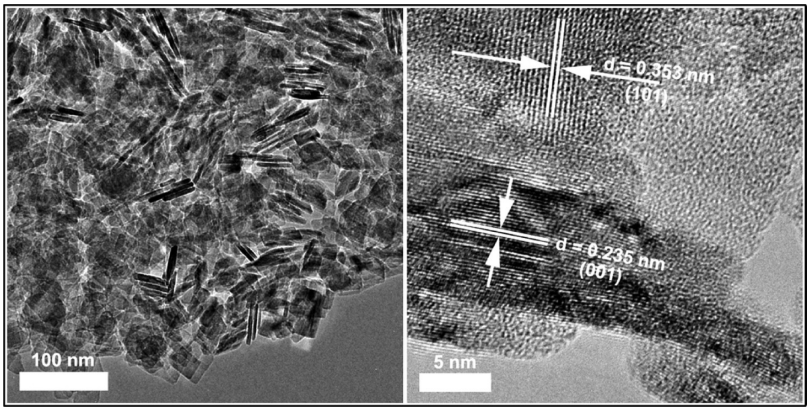

Figure 2. TEM and HRTEM images of 6HF-TiO_2.

samples was determined using the Barret–Joyner–Halender (BJH) method by obtaining their desorption isotherms. The concentration of surface OH groups was determined according to a saturated deprotonation method.[27−30]

2.3. Measurement of Photocatalytic Activity and Sample Analysis. The direct photolysis and photoreduction of Cr(VI) were carried out under simulated sunlight irradiation using a 500 W Xe arc lamp (Beijing Electric Light Sources Research Institute, Beijing, China) positioned 20 cm above a glass chamber reactor (10 cm diameter, 11 cm height, 500 mL total capacity) and surrounded by a self-contained water jacket. The solution was stirred continuously and the temperature of the suspension system was kept at 20 ± 1 °C by a water bath (THD-2015, Tianheng Instrument Factory, Ningbo, China) with flow through the surrounding water jacket.

In a typical run, 0.30 g of TiO_2 was suspended in 300 mL of aqueous solution of 15 mg L^{-1} $K_2Cr_2O_7$, followed by adjusting the pH to 3.0 with H_2SO_4 solution. Prior to irradiation, the suspensions were magnetically stirred in the dark for 30 min to ensure the establishment of adsorption–desorption equilibrium of Cr(VI) on the catalyst surface. At preset intervals, 5 mL aliquots were withdrawn, immediately centrifuged at 12,000 rpm for 5 min, and then filtered through a 0.45 μm membrane filter to remove the TiO_2 particles. The samples collected were then tested for Cr(VI) concentration using the standard DPC method.[31,32]

The concentration of soluble Cr(III) could be calculated by deducting the Cr(VI) concentration from the total Cr concentration in solution. The total Cr concentration was determined through oxidation of all soluble chromium forms into Cr(VI) by addition of excess $KMnO_4$ and subsequent detection of Cr(VI).[33]

3. RESULTS AND DISCUSSION

3.1. Characterization of Catalysts. *3.1.1. Morphology and Phase Structures.* FE–SEM is widely employed to obtain information on the morphological features and surface characteristics of the catalysts. The powder morphology and geometry of the resulting TiO_2 samples are depicted in Figure 1. The pure TiO_2 sample consisted of large numbers of aggregated nanoparticles. In contrast, the surface-fluorinated and fluorine-free (alkali-washed) samples displayed predominantly sheet-like structures with various side lengths and thicknesses. On the basis of this comparison, fluorine ions appear to play a significant role in the formation of TiO_2 nanosheets with high percentage of exposed {001} facets. The average side length distinctly increased from ∼40 to 150 nm when the initial HF volume was increased from 3 to 15 mL. The increase in length corresponds to a slight increase in the average thickness (from 10 to 15 nm), implying an increase of the proportion of the top and bottom areas with respect to the total surface area.[34,35] Accordingly, the percentage of {001} facets increased from 66% to 83%. Washing with 0.1 M NaOH solution did not markedly alter the percentage of (001) planes (Figure 1; Table 1).

TEM allows imaging of the crystallographic structure of a sample at an atomic scale. As shown in Figure 2, the representative 6HF-TiO_2 sample consisted of well-defined sheet structures having a rectangular outline. Further observation by high-resolution TEM (HRTEM) revealed a ∼0.235 nm lattice fringe parallel to the top and bottom facets, which could be assigned to the interplanar distance of the (001) planes of anatase TiO_2 (JCPDS 21-1272). The lattice space of the top surface was 0.353 nm in length, which was consistent

dx.doi.org/10.1021/ie400812m | Ind. Eng. Chem. Res. 2013, 52, 9556−9565

with the dimensions for the thermodynamically stable {101} facets (Figure 2). Therefore, the top and bottom facets of the nanosheets are the (001) and (00−1) planes, respectively.

The crystal shape, size, and percentage of TiO_2 facets exposed using the fluorination approach have been reported to depend on hydrothermal conditions such as reaction temperatures and F^- concentrations. The {100} and {001} facets could be formed preferentially at hydrothermal temperatures of 100−120 °C at a large range of F^- concentrations. In contrast, the {100} TiO_2 facet could not be formed by hydrothermal synthesis above 160 °C regardless of F^- concentration.[36] Our samples were prepared at a hydrothermal temperature of 180 °C. Therefore, the absence of observable {100} facets in the TEM images is reasonable. These results show an analogous morphology and are in agreement with the results of other studies.[22]

XRD can be used as an effective nondestructive tool for qualitative and quantitative analysis of the phase composition. As depicted in Figure 3, all TiO_2 samples showed peaks at 2θ

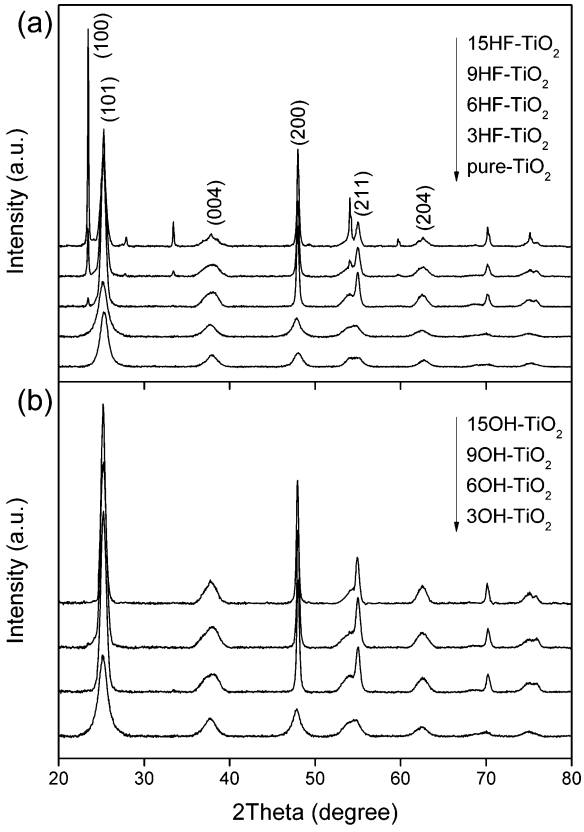

Figure 3. XRD patterns for pure-TiO_2, 3HF-TiO_2, 6HF-TiO_2, 9HF-TiO_2, 15HF-TiO_2, 3OH-TiO_2, 6OH-TiO_2, 9OH-TiO_2, and 15OH-TiO_2.

values of 25.3°, 38.2°, 48.1°, 55.0°, and 62.4°, corresponding to the anatase (101), (004), (200), (211), and (204) crystal planes (JCPDS 21-1272), respectively. In addition, the peak of the (100) crystalline phase of the surface-fluorinated samples ($TiOF_2$, JCPDS 08-0060) was visible, and its intensity increased with increasing HF concentration. The relative intensity of the peaks for the {100} facets of $TiOF_2$ diminished and then completely disappeared in the diffractograms of samples washed with 0.1 M NaOH. This trend indicates that all of the F in $TiOF_2$ is easily removed by alkali washing.

3.1.2. BET Surface Areas and Pore Size Distributions. Table 1 summarizes the quantitative details of the BET surface areas obtained from the nitrogen adsorption−desorption analysis. Pure-TiO_2 had the highest specific surface area (197 $m^2\ g^{-1}$). The trend of the BET surface areas of surface-fluorinated samples decreased (160 to 97 $m^2\ g^{-1}$) with the amount (3−15 mL) of the fluorinating agent. Similarly, the BET surface area of the fluorine-free catalysts decreased from 180 to 135 $m^2\ g^{-1}$. In addition, the specific surface area of samples washed with 0.1 M NaOH was always greater than that of the surface-fluorinated catalysts. This difference may be due to the ability of the alkali treatment to remove fluorine and to effectively clean the pores in HF-TiO_2.

The nitrogen adsorption−desorption isotherms and BJH pore size distributions derived from the desorption branch of the adsorption isotherms of the representative samples are shown in Figure 4. The isotherms of the fluorinated samples

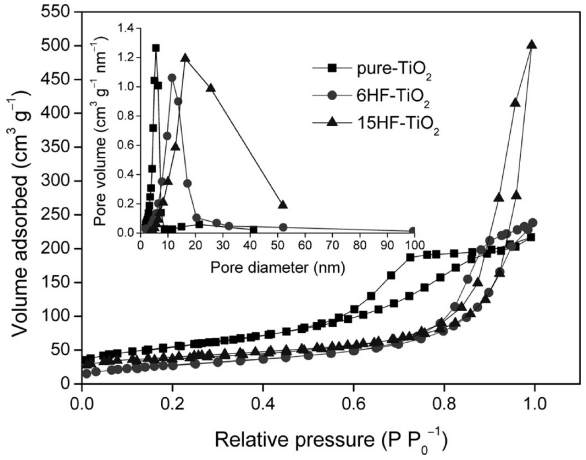

Figure 4. N_2 low-temperature adsorption−desorption isotherms and desorption pore size distribution plots for pure-TiO_2, 6HF-TiO_2, and 15HF-TiO_2.

have type IV patterns with type H3 hysteresis loops, according to the classification set forth by the International Union of Pure and Applied Chemistry.[37] These patterns are typical characteristics of mesoporous materials, and may originate from the randomly loose packing of the TiO_2 nanosheets. Well-defined H2 type hysteresis loops were observed in the pure-TiO_2 isotherms. The different types of hysteresis loops suggest that the pore shapes of the catalysts changed during the fluorination. Furthermore, the low end of the hysteresis loop in each isotherm corresponded to relative pressures of approximately 0.52, 0.55, and 0.60 for pure-TiO_2, 6HF-TiO_2, and 15HF-TiO_2, respectively. The fluorination appeared to lead to shifting of the hysteresis loops to higher relative pressures, which demonstrated that the pores were enlarged. Thus, the decreasing surface area with increasing initial HF concentration is ascribed to the loss of smaller pores. The BJH analysis of pore size distribution from the desorption branch of the isotherm also confirmed that the pore size of the three samples follow the order 15HF-TiO_2 > 6HF-TiO_2 > pure-TiO_2.

3.1.3. Surface Composition and Chemical State. XPS was used to inspect the change in the surface components and chemical states of TiO_2. The XPS survey spectrum of the surface-fluorinated TiO_2 nanosheets (Figure 5a) exhibits prominent peaks of C, Ti, O, and F. The XPS spectra of the Ti 2p core level region of all samples are shown in Figure 5b.

dx.doi.org/10.1021/ie400812m | Ind. Eng. Chem. Res. 2013, 52, 9556−9565

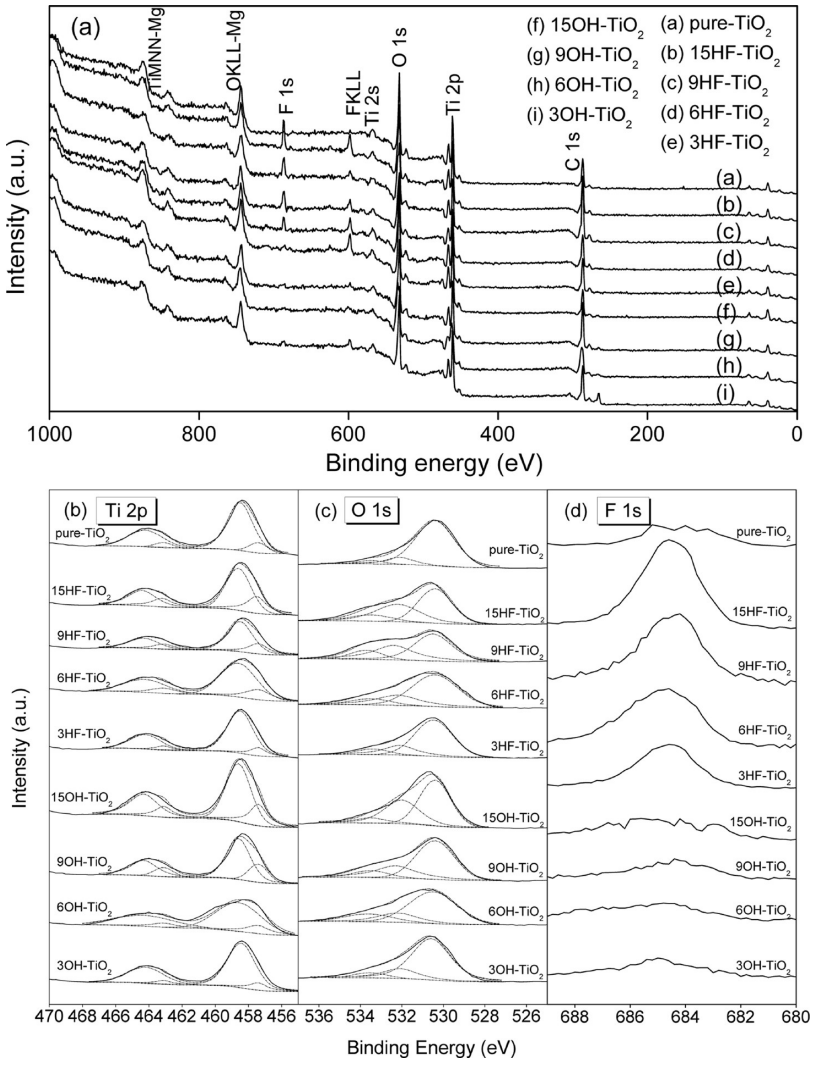

Figure 5. XPS spectra of (a) pure-TiO_2, 3HF-TiO_2, 6HF-TiO_2, 9HF-TiO_2, 15HF-TiO_2, 3OH-TiO_2, 6OH-TiO_2, 9OH-TiO_2, and 15OH-TiO_2; XPS spectra of the core levels of (b) Ti 2p, (c) O 1s, and (d) F 1s.

Table 2. Results of Fitting Data for the High-Resolution Spectra of the Ti 2p and O 1s Regions

		Ti−O−Ti		Ti−O−H		H−O−H	
samples	$Ti^{3+}/(Ti^{3+}+Ti^{4+})$ (%)	BE (eV)	area (%)	BE (eV)	area (%)	BE (eV)	area (%)
pure-TiO_2	13.9	530.4	85.8	532.1	10.5	533.5	3.7
3HF-TiO_2	16.6	530.5	68.6	532.1	22.5	533.4	9.0
6HF-TiO_2	26.9	530.4	62.9	532.2	26.8	533.5	1.3
9HF-TiO_2	34.7	530.5	50.5	532.4	37.1	533.7	12.4
15HF-TiO_2	44.6	530.4	50.1	532.2	39.0	533.5	10.8
3OH-TiO_2	14.2	530.6	74.8	532.1	18.7	533.5	6.5
6OH-TiO_2	21.0	530.5	64.4	532.2	20.0	533.6	15.6
9OH-TiO_2	31.8	530.4	46.5	532.2	37.4	533.3	16.2
15OH-TiO_2	35.5	530.4	53.6	532.0	37.3	533.5	9.1

The Ti 2p peaks at ~457.4 and 463.3 eV could be assigned to Ti^{3+}, and those at ~458.7 and 464.5 eV could be attributed to Ti^{4+}.[38,39] The curves were fitted using Gaussian symmetry, and the molar ratios of trivalent titanium to the sum of trivalent and tetravalent titanium, abbreviated here as $Ti^{3+}/(Ti^{3+} + Ti^{4+})$, were determined (Table 2). The $Ti^{3+}/(Ti^{3+} + Ti^{4+})$ ratio of the surface-fluorinated and fluorine-free (alkali-washed) samples increased with increasing initial F/Ti molar ratio, and the ratios of the surface-fluorinated catalyst samples were consistently higher than those of the alkali-washed samples. Trivalent titanium can be produced on the surface of TiO_2 by UV irradiation, annealing in vacuo, ion sputtering, plasma treatment, and ion doping.[40−43] In this work, Ti^{3+} should be produced from the charge compensation due to the added fluorine, which introduces an electron into the 3d orbital of Ti^{4+}. Additionally, creation of oxygen vacancies at the two-fold coordinated bridging sites results in the conversion of adjacent Ti^{4+} sites to Ti^{3+} defects. The Ti^{3+} in TiO_2 favors the

dx.doi.org/10.1021/ie400812m | Ind. Eng. Chem. Res. 2013, 52, 9556−9565

adsorption of oxygen and water molecules and thus promotes the generation of hydroxyl radicals.[44,45]

The high-resolution XPS spectra of the O1s region are illustrated in Figure 5c. Yaghoubi et al. identified two different O functional groups as well as a contribution of chemisorbed water in this region.[46] The peak at 530.5 eV is mainly assigned to the contribution of Ti−O−Ti in the TiO_2 crystal lattice, and the peak at 532.1 eV is closely related to Ti−O−H, which is considered to favor photocatalytic reactions. In addition, the binding energy of H−O−H bonds of the chemisorbed H_2O is 533.5 eV.[47] Similar to the change in the Ti^{3+} levels in TiO_2, the amount of surface Ti−O−H increased with increasing initial HF concentration. For instance, as the initial HF volume was increased from 3 to 15 mL, the ratio of Ti−O−H on HF-TiO_2 gradually increased from 22.5% to 39.0%. This corresponds to an increase (from 18.7% to 37.3%) in the Ti−O−H levels in the fluorine-free samples.

Figure 5d illustrates the high-resolution scan for F 1s, which contains only one peak at 684.6 eV. Generally, the F 1s range is composed of two peaks with binding energies of 687.8 and 684.7 eV, which are assigned to the substitutional F atoms in the TiO_2 crystal lattice and the ≡Ti−F species on the TiO_2 surface, respectively.[48,49] Therefore, the F atoms present on the surfaces were in the form of fluoride in this study. The absence of signals for F in the spectra of the alkali-treated samples further confirms that F on TiO_2 was present as a surface species.

3.2. Photocatalytic Activity. *3.2.1. Comparison of the Photocatalytic Activity of the Catalysts.* Figure 6 shows the photocatalytic reduction of aqueous Cr(VI) under UV−visible light irradiation in the presence and absence of the as-synthesized TiO_2. No reduction of Cr(VI) was detected when the sample was irradiated in the absence of the catalyst, indicating that the direct photolysis scarcely contributed to the photocatalytic reduction of Cr(VI). Instead, the pure-TiO_2 catalyst synthesized in pure water displayed high photocatalytic activity. Moreover, the activity of all TiO_2 nanosheets was considerably higher than that of pure-TiO_2. In particular, 6HF-TiO_2 achieved a maximum reduction percentage of 96% after 60 min reaction under simulated sunlight irradiation, which is much higher than that for the pure-TiO_2 (33%). To quantitatively compare photocatalytic activities, the reaction rate constant (k) for the photocatalytic reduction of Cr(VI) over the samples was evaluated using the pseudo-first-order model:[50]

$$\ln\left(\frac{C_0}{C_t}\right) = kt \tag{4}$$

where C_0 and C_t are the concentrations of aqueous Cr(VI) after illumination for 0 and t min, respectively. The results for fitting data for the Cr(VI) reduction kinetics to the model are listed in Table 1. The calculated rate constants are 7.6×10^{-3}, 2.62×10^{-2}, 5.37×10^{-2}, 4.46×10^{-2}, and 3.42×10^{-2} min^{-1} for the catalysts pure-TiO_2, 3HF-TiO_2, 6HF-TiO_2, 9HF-TiO_2, and 15HF-TiO_2, respectively. This trend indicates that the order of catalytic activity is pure-TiO_2 < 3HF-TiO_2 < 15HF-TiO_2 < 9HF-TiO_2 < 6HF-TiO_2. The reaction rates for all fluorine-free catalysts follow the same trend as those for the surface-fluorinated samples: the pseudo-first-order rate constants were 8.1×10^{-3}, 3.72×10^{-2}, 1.92×10^{-2}, and 1.10×10^{-2} min^{-1} for the catalysts 3OH-TiO_2, 6OH-TiO_2, 9OH-TiO_2, and 15OH-TiO_2, respectively. Furthermore, the lower photocatalytic activity of the fluorine-free samples compared with that of the corresponding surface-fluorinated catalysts confirm the enhancement of the photocatalytic reduction of Cr(VI) by surface fluorination.

The variation in the photocatalytic activity of TiO_2 may be explained by the combined action of factors such as particle size, specific surface area, band gap, crystal phase, morphology, surface chemical state and composition, crystallinity, and crystal defects. As mentioned, the main differences in the physicochemical properties of catalysts arise from differences in their surface chemistry and morphology. Hence, the decreasing trend described above could be partly explained by the influence of the surface fluorination and the percentage of {001} facets of TiO_2 on the photocatalytic reduction of Cr(VI).

3.2.2. Effect of {001} Facets and Surface Fluorination of TiO_2 on the Adsorption of Cr(VI). It is widely known that photocatalytic Cr(VI) reduction occurs on the surface of the photocatalyst.[8,51] Therefore, Cr(VI) adsorption on the surface is required for the photocatalytic process. In this study, the pH (3.0) of the aqueous suspension of TiO_2 upon acidification with H_2SO_4 was lower than the zero point of charge (pH_{PZC}) of TiO_2. Thus, the negatively charged $Cr_2O_7^{2-}$ could have electrostatic interactions with the positively charged $TiOH_2^+$ groups on the TiO_2 surfaces, leading to adsorption. The mechanism of adsorption of dichromate on the surface of TiO_2 via the active groups can be expressed by the following equations:[52,53]

$$TiOH + H^+ \rightarrow TiOH_2^+ \quad (pH < pH_{PZC}) \tag{5}$$

$$TiOH + OH^- \rightarrow TiO^- + H_2O \quad (pH > pH_{PZC}) \tag{6}$$

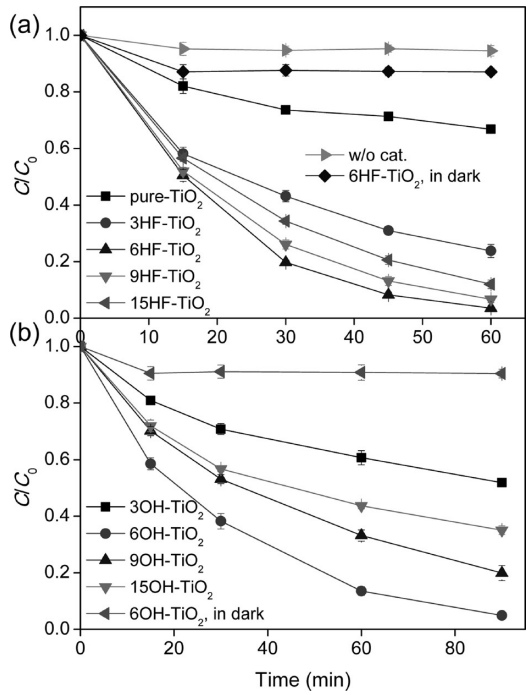

Figure 6. Plots of the $K_2Cr_2O_7$ concentration vs irradiation time in the presence of various photocatalysts and in the absence of photocatalysts under UV−visible light irradiation; similar plots in the presence of 6HF-TiO_2 and 6OH-TiO_2 in darkness. Initial concentration of $K_2Cr_2O_7$, 15 mg L^{-1}; catalyst dose, 1.0 g L^{-1}; reaction temperature, 20 °C.

dx.doi.org/10.1021/ie400812m | Ind. Eng. Chem. Res. 2013, 52, 9556−9565

$$TiOH_2^+ + Cr_2O_7^{2-} \rightarrow TiOHCr_2O_7^{2-} + H^+ \quad (7)$$

As shown by these equations, the number of surface OH groups plays a decisive role in the photocatalytic reduction of Cr(VI). An increase in the concentration of surface OH groups would enhance the generation of $TiOHCr_2O_7^{2-}$ (eq 7) and therefore provide a high-concentration reaction environment for the photocatalytic reaction (eq 2). In this study, the amount of OH groups on the TiO_2 surface was determined to acquire detailed information on their relationship to the photocatalytic activity; results of these analyses are given in Table 1.

For the pure-TiO_2, 3OH-TiO_2, 6OH-TiO_2, 9OH-TiO_2, and 15OH-TiO_2 samples, increasing the percentage of {001} facets of TiO_2 from 10% to 83% resulted in a significant increase (from 0.825 to 2.190 mg g^{-1}) of $Cr_2O_7^{2-}$ adsorbed. In particular, the higher the percentage of {001} facets, the more the adsorption of Cr(VI) reached saturation levels. Direct dissociation of H_2O has been reported to occur at oxygen vacancy sites of the (001) surface of TiO_2. This association leads to generation of OH groups, and the remaining H atom donated from H_2O reacts with lattice oxygen to produce another hydroxyl radical.[54−56] As a consequence, the high percentage of exposed {001} facets facilitated the adsorption of Cr(VI) on the surface.

The FESEM results demonstrate that the crystal structure and morphology of TiO_2 as well as the percentage of {001} facets were almost the same before and after alkali washing. Thus, the role of fluorination in Cr(VI) adsorption could be evaluated by subtracting the effect of the facets. Taking into account the results in Table 1, the surface fluorination can be assumed to have a significant influence on the adsorption of $Cr_2O_7^{2-}$. The saturated adsorption capacity of the HF-TiO_2 catalysts was approximately 20−40% higher than that of the coupled OH-TiO_2 samples.

The concentration of surface OH groups is correlated with the number of Ti^{3+} sites. This correlation can be explained by the tendency of oxygen and water molecules to be adsorbed on the Ti^{3+} sites, which are more hydrophilic than the Ti^{4+} sites of TiO_2; consequently, the binding accelerates the formation of surface OH groups.[44,45] From the XPS analysis, the $Ti^{3+}/(Ti^{3+} + Ti^{4+})$ ratio of HF-TiO_2 was found to be 10−35% higher than that of OH-TiO_2. In this case, F^- on the surface of TiO_2 was removed by a simple ligand exchange reaction between OH^- in the NaOH solution and F^- on TiO_2.[22] Corroborating this result, the anatase TiO_2 catalysts with surface fluorination, which contained more Ti^{3+} and surface OH groups, showed more efficient adsorption of Cr(VI) in aqueous medium.

In summary, the increased adsorption of Cr(VI) onto TiO_2 can be mainly ascribed to the synergetic enhancement by the exposure of highly reactive {001} facets of nanosheets and their surface fluorination.

3.2.3. Effect of the Percentage of {001} Facets and Surface Fluorination of TiO_2 on the Reduction Reaction of Cr(VI). The following discussion focuses on the influence of the percentage of {001} facets and surface fluorination of TiO_2 on the photocatalytic reaction. Under UV−visible illumination, reduction of Cr(VI) occurred by direct capture of photogenerated electrons from the surface Ti^{3+} of the TiO_2 photocatalyst (eq 2). Since no other reducing agents or hole scavengers were added, the photoreduction of Cr(VI) is accompanied by oxidation of water to give O_2 with photogenerated holes (eq 3). As reported, the rate-determining step for the photocatalytic reduction of Cr(VI) is the surface reaction after Cr(VI) is adsorbed on TiO_2.[8] Hence, the photocatalytic activity may depend on the surface physicochemical characteristics of the photocatalysts. To investigate the effect of the crystal face of TiO_2 on the reduction of Cr(VI) under UV−visible irradiation and to exclude the effect of the surface fluorination, the catalysts 3OH-TiO_2, 6OH-TiO_2, 9OH-TiO_2, and 15OH-TiO_2, which represent various {001} facet compositions, were chosen for study. As can be seen in Table 1, when the initial F/Ti ratio was varied from 0 to 1, a higher percentage of {001} facets led to increasing values of k. In particular, the constants 7.6×10^{-3}, 8.1×10^{-3}, and 3.72×10^{-2} min^{-1} correspond to the proportions of {001} facets 10%, 65%, and 72%, respectively. However, a further increase (from 1 to 2.67) in the F/Ti ratio was associated with a reduction in the photocatalytic reaction rate; the pseudo-first-order rate constant decreased from 3.72×10^{-2} to 1.10×10^{-2} min^{-1}. In other words, 6OH-TiO_2 possessed an optimal percentage (~72%) of anatase {001} facets, which resulted in the highest photocatalytic activity.

The profound dependence of the various physicochemical properties of TiO_2 on the facets present on its surface is a behavior typical of the fundamental anisotropy of crystals.[57] Density functional theory calculations predicted that the conduction band potential of anatase (101) is slightly lower than that of anatase (001). Therefore, the {101} facets serve as reservoirs of the photogenerated electrons for the TiO_2 nanocrystals enclosed with {101} and {001} facets, whereas photogenerated holes are concentrated on the {001} facets.[23,58] This prediction result was verified by Ohno et al. via photodeposition of Pt and PbO_2.[59] In other words, the {001} and {101} facets of anatase TiO_2 usually act as oxidative and reductive sites that trap photogenerated holes and electrons, leading to oxidation and reduction on the {001} and {101} facets, respectively.[59−61] Thus, we inferred that the oxidation of water to O_2 (eq 3) mainly occurs on the {001} facets, inevitably coinciding with the reduction of Cr(VI) to Cr(III) (eq 2) on the {101} facets. Therefore, a balance between the redox reactions must be achieved for optimal photocatalytic activity. In this study, increasing the percentage of {001} facets favors the transfer of photogenerated holes to water, thereby reducing the recombination rate of the photoexcited electron−hole pairs and leaving more electrons for the reduction of Cr(VI) on the {101} facets. However, an increase in the amount of the exposed {001} facets corresponded to a decrease in the number of {101} facets, which retarded the Cr(VI) reduction. Accordingly, an optimal ratio of the oxidative {001} facets to the reductive {101} facets is required to balance the redox reaction rates and recombination rates of photogenerated electrons and holes during photocatalysis on the TiO_2 nanosheets. From the results, we demonstrate that TiO_2 with an appropriate ratio of {001} to {101} facets (approximately 72:18) possesses higher photocatalytic activity compared with that of the other samples. A similar phenomenon wherein an optimal ratio of the amount of oxidative {001} facets to that of the reductive {101} facets has been observed by other researchers who used faceted TiO_2 nanocrystals as photocatalysts.[23,59]

Surface fluorination is another important factor that determines photocatalytic activity. In our experiments, Cr(VI) was reduced much faster on fluorinated samples than on the nonfluorinated samples, as evident in the 1.5−3-fold increase in the reaction rate constant (Table 1). Because of its high electronegativity, fluorine in the surface ≡Ti−F group may

dx.doi.org/10.1021/ie400812m | Ind. Eng. Chem. Res. 2013, 52, 9556−9565

favor electron trapping, thereby suppressing the recombination of photogenerated electron−hole pairs.[62]

Briefly, we conclude that surface fluorination is helpful to accelerate the reaction rate of the photocatalytic reduction of Cr(VI), and that an appropriate ratio of {001} to {101} facets enhances the catalytic activity of TiO_2. Since {001} facet is the major active-site where oxidation of water to O_2 occurs, the enhancement of the Cr(VI) adsorption on TiO_2 by increasing the percentage of {001} facets seems to play an insignificant role in the photocatalytic reduction of Cr(VI) in aqueous solution.

3.2.4. Balance of Cr in Aqueous Solution. A mass balance analysis of the Cr is required to obtain a better understanding of the photocatalytic mechanism. It can be seen from Figure 7

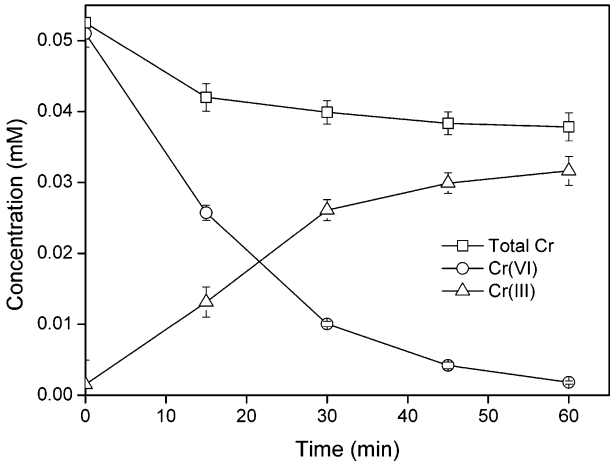

Figure 7. Time profile of the change in Cr concentration in aqueous solution during the photocatalytic reduction of $K_2Cr_2O_7$ over 6HF-TiO_2 catalysts under UV−visible light irradiation. Initial concentration of $K_2Cr_2O_7$, 15 mg L^{-1}; catalyst dose, 1.0 g L^{-1}; reaction temperature, 20 °C.

that the molar concentration of the Cr(III) produced was less than that of the Cr(VI) reduced by using 6HF-TiO_2 as photocatalyst. We therefore infer that the loss of Cr is caused by the residual adsorption of Cr(VI) on the photocatalysts, in which Cr(VI) has not been rapidly reduced photocatalytically. Furthermore, the deposition of Cr(III) on the TiO_2 surface in the form of $Cr(OH)_3$ could also result in a deficit in the Cr balance.[53] It should be noted that the adsorbed $Cr(OH)_3$ could be removed by reacting it with NaOH, thereby forming $Cr(OH)_4^-$. Tuprakay and Liengcharernsit demonstrated that the spent TiO_2 could be regenerated by washing off the $Cr(OH)_3$ with 3 M NaOH.[53]

4. CONCLUSIONS

The photoreduction of Cr(VI) was investigated using surface-fluorinated anatase TiO_2 nanosheets, the exposed facets of which consisted chiefly of {001} facets. In aqueous media, the fluorinated TiO_2 nanosheets showed higher catalytic activity for Cr(VI) reduction than did pure-TiO_2. The enhanced catalytic activity is due to the synergistic effect of surface fluorination and exposed {001} facets on the adsorption capacity and photoactivity of TiO_2. The highest catalytic activity was exhibited by the 6HF-TiO_2, which afforded a rate constant 7 times greater than that achieved using pure-TiO_2. In addition, all fluorinated TiO_2 nanosheet samples demonstrated 1.5−3 times higher photocatalytic activity than did the nonfluorinated TiO_2. The increased activity suggests that the presence of F^- on the TiO_2 surface favors the photoreduction of Cr(VI).

We conclude that a proper ratio of {001} to {101} facets increases the reduction rate of Cr(VI) by enhancing the oxidation of water to O_2. Surface fluorination not only leads to a marked rise in the rate of Cr(VI) adsorption but also hinders the recombination of the photoexcited electron−hole pairs.

Further improvements in the physicochemical properties of the TiO_2 catalyst may ultimately lead to a suitable candidate for the photocatalytic reduction of other substances in water.

AUTHOR INFORMATION

Corresponding Author

*Tel.: 86-571-88320726. Fax: 86-571-88320276. E-mail: ss@zjut.edu.cn.

Notes

The authors declare no competing financial interest.

ACKNOWLEDGMENTS

This work was supported by the National Natural Science Foundation of China (Grant Nos. 20977086, 21076196, and 21177115), and the Zhejiang Provincial Natural Science Foundation of China (LR13B070002).

REFERENCES

(1) Wang, X. L.; Phekonen, S. O.; Ray, A. K. Removal of aqueous Cr(VI) by a combination of photocatalytic reduction and coprecipitation. *Ind. Eng. Chem. Res.* **2004**, *43*, 1665−1672.

(2) Meichtry, J. M.; Brusa, M.; Mailhot, G.; Grela, M. A.; Litter, M. I. Heterogeneous photocatalysis of Cr(VI) in the presence of citric acid over TiO_2 particles: Relevance of Cr(V)−citrate complexes. *Appl. Catal., B* **2007**, *71*, 101−107.

(3) Jiang, F.; Zheng, Z.; Xu, Z. Y.; Zheng, S. R.; Guo, Z. B.; Chen, L. Q. Aqueous Cr(VI) photo-reduction catalyzed by TiO_2 and sulfated TiO_2. *J. Hazard. Mater.* **2006**, *B134*, 94−103.

(4) Yang, J. K.; Lee, S. M. Removal of Cr(VI) and humic acid by using TiO_2 photocatalysis. *Chemosphere* **2006**, *63*, 1677−1684.

(5) Testa, J. J.; Grela, M. A.; Litter, M. I. Heterogeneous photocatalytic reduction of chromium(VI) over TiO_2 particles in the presence of oxalate: involvement of Cr(V) species. *Environ. Sci. Technol.* **2004**, *38*, 1589−1594.

(6) Yang, M.; Zhang, Y. C.; Dai, W. M.; Hang, K.; Pan, Y. Q. Synthesis of SnS_2/SnO_2 nanocomposite for visible light-driven photocatalytic reduction of aqueous Cr(VI). *Key Eng. Mater* **2013**, *538*, 46−49.

(7) Gu, B. H.; Chen, J. Enhanced microbial reduction of Cr(VI) and U(VI) by different natural organic matter fractions. *Geochim. Cosmochim. Acta.* **2003**, *67*, 3575−3582.

(8) Ku, Y.; Jung, I. L. Photocatalytic reduction of Cr(VI) in aqueous solutions by UV irradiation with the presence of titanium dioxide. *Water Res.* **2001**, *35*, 135−142.

(9) Asuha, S.; Zhou, X. G.; Zhao, S. Adsorption of methyl orange and Cr(VI) on mesoporous TiO_2 prepared by hydrothermal method. *J. Hazard. Mater.* **2010**, *181*, 204−210.

(10) Testa, J. J.; Grela, M. A.; Litter, M. I. Experimental evidence in favor of an initial one-electron-transfer process in the heterogeneous photocatalytic reduction of chromium(VI) over TiO_2. *Langmuir* **2001**, *17*, 3515−3517.

(11) Wang, L. M.; Wang, N.; Zhu, L. H.; Yu, H. W.; Tang, H. Q. Photocatalytic reduction of Cr(VI) over different TiO_2 photocatalysts and the effects of dissolved organic species. *J. Hazard. Mater.* **2008**, *152*, 93−99.

(12) Li, X. Z.; Li, F. B. Study of Au/Au^{3+}-TiO_2 photocatalysts toward visible photooxidation for water and wastewater treatment. *Environ. Sci. Technol.* **2001**, *35*, 2381−2387.

(13) Rao, A. R.; Dutta, V. Low-temperature synthesis of TiO_2 nanoparticles and preparation of TiO_2 thin films by spray deposition. *Sol. Energy Mater. Sol. Cells* **2007**, *91*, 1075−1080.
(14) Liu, G.; Yu, J. C.; Lu, G. Q.; Cheng, H. M. Crystal facet engineering of semiconductor photocatalysts: Motivations, advances and unique properties. *Chem. Commun.* **2011**, *47*, 6763−6783.
(15) Lv, K. L.; Cheng, B.; Yu, J. G.; Liu, G. Fluorine ions-mediated morphology control of anatase TiO_2 with enhanced photocatalytic activity. *Phys. Chem. Chem. Phys.* **2012**, *14*, 5349−5362.
(16) Tanaka, K. I.; Blyholder, G. Photocatalytic reactions on semiconductor surfaces. I. Decomposition of nitrous oxide on zinc oxide. *J. Phys. Chem.* **1971**, *75*, 1037−1043.
(17) Liu, M.; Piao, L. Y.; Zhao, L.; Ju, S. T.; Yan, Z. J.; He, T.; Zhou, C. L.; Wang, W. J. Anatase TiO_2 single crystals with exposed {001} and {110} facets: facile synthesis and enhanced photocatalysis. *Chem. Commun.* **2010**, *46*, 1664−1666.
(18) Gong, X. Q.; Selloni, A. Reactivity of anatase TiO_2 nanoparticles: the role of the minority (001) surface. *J. Phys. Chem. B* **2005**, *109*, 19560−19562.
(19) Lazzeri, M.; Vittadini, A.; Selloni, A. Structure and energetics of stoichiometric TiO_2 anatase surfaces. *Phys. Rev. B* **2002**, *65*, 119901.
(20) Yang, H. G.; Sun, C. H.; Qiao, S. Z.; Zou, J.; Liu, G.; Smith, S. C.; Cheng, H. M.; Lu, G. Q. Anatase TiO_2 single crystals with a large percentage of reactive facets. *Nature* **2008**, *453*, 638−642.
(21) Wang, W.; Ni, Y. R.; Lu, C. H.; Xu, Z. Z. Hydrogenation of TiO_2 nanosheets with exposed {001} facets for enhanced photocatalytc activity. *RSC Adv.* **2012**, *2*, 8286−8288.
(22) Xiang, Q. J.; Lv, K.; Yu, J. G. Pivotal role of fluorine in enhanced photocatalytic activity of anatase TiO_2 nanosheets with dominant (001) facets for the photocatalytic degradation of acetone in air. *Appl. Catal., B* **2010**, *96*, 557−564.
(23) Liu, C.; Han, X. G.; Xie, S. F.; Kuang, Q.; Wang, X.; Jin, M. S.; Xie, Z. X.; Zheng, L. S. Enhancing the photocatalytic activity of anatase TiO_2 by improving the specific facet-induced spontaneous separation of photogenerated electrons and holes. *Chem.—Asian J.* **2013**, *8*, 282−289.
(24) Arrouvel, C.; Digne, M.; Breysse, M.; Toulhoat, H.; Raybaud, P. Effects of morphology on surface hydroxyl concentration: A DFT comparison of anatase-TiO_2 and γ-alumina catalytic supports. *J. Catal.* **2004**, *222*, 152−166.
(25) Yu, J. G.; Xiang, Q. J.; Ran, J. R.; Mann, S. One-step hydrothermal fabrication and photocatalytic activity of surface-fluorinated TiO_2 hollow microspheres and tabular anatase single micro-crystals with high-energy facets. *CrystEngComm* **2010**, *12*, 872−879.
(26) Han, X. G.; Kuang, Q.; Jin, M. S.; Xie, Z. X.; Zheng, L. S. Synthesis of titania nanosheets with a high percentage of exposed (001) facets and related photocatalytic properties. *J. Am. Chem. Soc.* **2009**, *131*, 3152−3153.
(27) He, Z. Q.; Cai, Q. L.; Hong, F. Y.; Jiang, Z.; Chen, J. M.; Song, S. Effective enhancement of the degradation of oxalic acid by catalytic ozonation with TiO_2 by exposure of {001} facets and surface fluorination. *Ind. Eng. Chem. Res.* **2012**, *51*, 5662−5668.
(28) Laiti, E.; Öhman, L. O.; Nordin, J.; Sjöberg, S. Acid/base properties and phenylphosphonic acid complexation at the aged γ-Al_2O_3/water interface. *J. Colloid Interface Sci.* **1995**, *175*, 230−238.
(29) Tamura, H.; Tanaka, A.; Mita, K.; Furuichi, R. Surface hydroxyl site densities on metal oxides as a measure for the ion-exchange capacity. *J. Colloid Interface Sci.* **1999**, *209*, 225−231.
(30) Xiang, Q. J.; Yu, J. G.; Wong, P. K. Quantitative characterization of hydroxyl radicals produced by various photocatalysts. *J. Colloid Interface Sci.* **2011**, *357*, 163−167.
(31) Idris, A.; Hassan, N.; Rashid, R.; Ngomsik, A. F. Kinetic and regeneration studies of photocatalytic magnetic separable beads for chromium (VI) reduction under sunlight. *J. Hazard. Mater.* **2011**, *186*, 629−635.
(32) Zakaria, Z. A.; Zakaria, Z.; Surif, S.; Ahmad, W. A. Hexavalent chromium reduction by Acinetobacter haemolyticus isolated from heavy-metal contaminated wastewater. *J. Hazard. Mater.* **2007**, *146*, 30−38.
(33) Cheng, Y. J.; Yan, F. B.; Huang, F.; Chu, W. S.; Pan, D. M.; Chen, Z.; Zheng, J. S.; Yu, M. J.; Lin, Z.; Wu, Z. Y. Bioremediation of Cr(VI) and immobilization as Cr(III) by *Ochrobactrum anthropi*. *Environ. Sci. Technol.* **2010**, *44*, 6357−6363.
(34) Xiang, Q. J.; Yu, J. G.; Jaroniec, M. Tunable photocatalytic selectivity of TiO_2 films consisted of flower-like microspheres with exposed {001} facets. *Chem. Commun.* **2011**, *47*, 4532−4534.
(35) Lazzeri, M.; Vittadini, A.; Selloni, A. Structure and energetics of stoichiometric TiO_2 anatase surfaces. *Phys. Rev. B* **2001**, *63*, 155409.
(36) Lai, Z. C.; Peng, F.; Wang, Y.; Wang, H. J.; Yu, H.; Liu, P. R.; Zhao, H. J. Low temperature solvothermal synthesis of anatase TiO_2 single crystals with wholly {100} and {001} faceted surfaces. *J. Mater. Chem.* **2012**, *22*, 23906−23912.
(37) Sing, K. S. W.; Everett, D. H.; Haul, R. A. W.; Moscou, L.; Pierotti, R. A.; Rouquerol, J.; Siemieniewska, T. Reporting physisorption data for gas/solid systems with special reference to the determination of surface area and porosity. *Pure Appl. Chem.* **1985**, *57*, 603−619.
(38) Chen, S. C.; Sung, K. Y.; Tzeng, W. Y.; Wu, K. H.; Juang, J. Y.; Uen, T. M.; Luo, C. W.; Lin, J. Y.; Kobayashi, T.; Kuo, H. C. Microstructure and magnetic properties of oxidized titanium nitride thin films in situ grown by pulsed laser deposition. *J. Phys. D: Appl. Phys.* **2013**, *46*, 075002.
(39) Cheng, Y. P.; Sun, H. Q.; Jin, W. Q.; Xu, N. P. Photocatalytic degradation of 4-chlorophenol with combustion synthesized TiO_2 under visible light irradiation. *Chem. Eng. J.* **2007**, *128*, 127−133.
(40) Hengerer, R.; Bolliger, B.; Erbudak, M.; Gratzel, M. Structure and stability of the anatase TiO_2 (101) and (001) surfaces. *Surf. Sci.* **2000**, *460*, 162−169.
(41) Guillemot, F.; Porte, M. C.; Labrugere, C.; Baquey, C. Ti^{4+} to Ti^{3+} conversion of TiO_2 uppermost layer by low-temperature vacuum annealing: Interest for titanium biomedical applications. *J. Colloid Interface Sci.* **2002**, *255*, 75−78.
(42) Liu, H. M.; Yang, W. S.; Ma, Y.; Cao, Y.; Yao, J. N.; Zhang, J.; Hu, T. D. Synthesis and characterization of titania prepared by using a photoassisted sol-gel method. *Langmuir* **2003**, *19*, 3001−3005.
(43) Suriye, K.; Praserthdam, P.; Jongsomjit, B. Control of Ti^{3+} surface defect on TiO_2 nanocrystal using various calcinations atmospheres as the first step for surface defect creation and its application in photocatalysis. *Appl. Surf. Sci.* **2007**, *253*, 3849−3855.
(44) Wang, X. P.; Yu, Y.; Hu, X. F.; Gao, L. Hydrophilicity of TiO_2 films prepared by liquid phase deposition. *Thin Solid Films* **2000**, *371*, 148−152.
(45) Jung, J. M.; Wang, M.; Kim, E. J.; Hahn, S. H. Photocatalytic properties of Au/TiO_2 thin films prepared by RF magnetron cosputtering. *Vacuum* **2008**, *82*, 827−832.
(46) Tang, X. L.; Li, K.; Yi, H. H.; Ning, P.; Xiang, Y.; Wang, J. G.; Wang, C. MnOx catalysts modified by nonthermal plasma for no catalytic oxidation. *J. Phys. Chem. C* **2012**, *116*, 10017−10028.
(47) Yaghoubi, H.; Taghavinia, N.; Alamdari, E. K.; Volinsky, A. A. Nanomechanical properties of TiO_2 granular thin films. *ACS Appl. Mater. Interfaces* **2010**, *2*, 2629−2636.
(48) Li, D.; Haneda, H.; Hishita, S.; Ohashi, N.; Labhsetwar, N. K. Fluorine-doped TiO_2 powders prepared by spray pyrolysis and their improved photocatalytic activity for decomposition of gas-phase acetaldehyde. *J. Fluorine Chem.* **2005**, *126*, 69−77.
(49) Li, D.; Ohashi, N.; Hishita, S.; Kolodiazhnyi, T.; Haneda, H. Origin of visible-light-driven photocatalysis: A comparative study on N/F-doped and N-F-codoped TiO_2 powders by means of experimental characterizations and theoretical calculations. *J. Solid State Chem.* **2005**, *178*, 3293−3302.
(50) Sarwan, B.; Pare, B.; Acharya, A. D.; Jonnalagadda, S. B. Mineralization and toxicity reduction of textile dye neutral red in aqueous phase using BiOCl photocatalysis. *J. Photochem. Photobiol. B* **2012**, *116*, 48−55.
(51) Yang, J.; Dai, J.; Li, J. T. Visible-light-induced photocatalytic reduction of Cr(VI) with coupled Bi_2O_3/TiO_2 photocatalyst and the

synergistic bisphenol A oxidation. *Environ. Sci. Pollut. Res.* **2013**, *20*, 2435−2447.
(52) Zhao, L.; Sun, Z. Z.; Ma, J. Novel relationship between hydroxyl radical initiation and surface group of ceramic honeycomb supported metals for the catalytic ozonation of nitrobenzene in aqueous solution. *Environ. Sci. Technol.* **2009**, *43*, 4157−4163.
(53) Tuprakay, S.; Liengcharernsit, W. Lifetime and regeneration of immobilized titania for photocatalytic removal of aqueous hexavalent chromium. *J. Hazard. Mater.* **2005**, *B124*, 53−58.
(54) Bustillo, F. J.; Roman, E.; de Segovia, J. L. Adsorption and thermal desorption of H_2O on TiO_2 (001) at 250 K. *Vacuum* **1989**, *39*, 659−661.
(55) Namai, Y.; Matsuoka, O. Chain structures of surface hydroxyl groups formed via line oxygen vacancies on TiO_2 (110) surfaces studied using noncontact atomic force microscopy. *J. Phys. Chem. B* **2005**, *109*, 23948−23954.
(56) Bonapasta, A. A.; Filippone, F.; Mattioli, G.; Alippi, P. Oxygen vacancies and OH species in rutile and anatase TiO_2 polymorphs. *Catal. Today* **2009**, *144*, 177−182.
(57) Teoh, W. Y.; Scott, J. A.; Amal, R. Progress in heterogeneous photocatalysis: From classical radical chemistry to engineering nanomaterials and solar reactors. *J. Phys. Chem. Lett.* **2012**, *3*, 629−639.
(58) Tachikawa, T.; Yamashita, S.; Majima, T. Evidence for crystal-face-dependent TiO_2 photocatalysis from single-molecule imaging and kinetic analysis. *J. Am. Chem. Soc.* **2011**, *133*, 7197−7204.
(59) Murakami, N.; Kurihara, Y.; Tsubota, T.; Ohno, T. Shape-controlled anatase titanium(IV) oxide particles prepared by hydrothermal treatment of peroxo titanic acid in the presence of polyvinyl alcohol. *J. Phys. Chem. C* **2009**, *113*, 3062−3069.
(60) Ohno, T.; Sarukawa, K.; Matsumura, M. Crystal faces of rutile and anatase TiO_2 particles and their roles in photocatalytic reactions. *New J. Chem.* **2002**, *26*, 1167−1170.
(61) Taguchi, T.; Saito, Y.; Sarukawa, K.; Ohno, T.; Matsumura, M. Formation of new crystal faces on TiO_2 particles by treatment with aqueous HF solution or hot sulfuric acid. *New J. Chem.* **2003**, *27*, 1304−1306.
(62) Yu, J. G.; Wang, W. G.; Cheng, B.; Su, B. L. Enhancement of photocatalytic activity of mesporous TiO_2 powders by hydrothermal surface fluorination treatment. *J. Phys. Chem. C* **2009**, *113*, 6743−6750.